Solar Energy Materials & Solar Cells 107 (2012) 69–74

Contents lists available at SciVerse ScienceDirect

Solar Energy Materials & Solar Cells

journal homepage: www.elsevier.com/locate/solmat

Effects of metal-free conjugated oligomer as a surface modifier in hybrid polymer/ZnO solar cells

Chiang-Ting Chen [a], Fang-Chi Hsu [b,*], Yun-Ming Sung [a], Hsueh-Chung Liao [c], Wei-Che Yen [c], Wei-Fang Su [c], Yang-Fang Chen [a,*]

[a] Department of Physics, National Taiwan University, Taipei 106, Taiwan
[b] Department of Materials Science and Engineering, National United University, Miaoli 360, Taiwan
[c] Department of Materials Science and Engineering, National Taiwan University, Taipei 106, Taiwan

ARTICLE INFO

Article history:
Received 29 March 2012
Received in revised form
16 July 2012
Accepted 2 August 2012
Available online 31 August 2012

Keywords:
Hybrid solar cell
ZnO
Interface
Surface modification
Oligomer
Transport

ABSTRACT

The interface property has been one of the critical issues in developing hybrid polymer/metal oxide solar cells. We synthesize a conjugated oligomer, an amine- and bromine-terminated 3-hexyl thiophene (O3HT-(Br)NH_2), to modify the ZnO-nanorod (ZnO-NR) surface in hybrid polymer/ZnO-NR photovoltaic cells. This oligomer is of the same repeat unit structure as and ~1/12 the contour length of that of the light-harvesting polymer. In addition to passivate the NR surface, the presence of this conjugated oligomer enhances the electron mobility, and drives larger hole density toward the anodic surface for collection. The improved charge transport property of the hybrid is presumably a result of modulating the nanomorphology of the bi-carrier transport network induced by the conjugated oligomer. As a result, there is a large enhancement in photocurrent and photovoltage leading to an improved device performance of ~35%.

1. Introduction

Polymer based solar cells (PSCs) have received considerable attentions by scientists for the past decade because of being considered as a promising alternative for low-cost energy device production [1–5]. A typical approach used to integrate polymer materials in PSC is to employ the bulk heterojunction (BHJ) concept [6–10], in which the donor and acceptor materials are closely intermixed in a nanometer scale. In the BHJ structure, there is a large interfacial area created beneficial for exciton dissociation; however, the resulting interpenetration charge transport network formed by donor and acceptor phases is bi-continuous. Under such a condition, electron (hole) traveling pathway is indirect and uncontrollable, and this morphological nature could be detrimental to the carrier mobility as compared to the system of ordered transport paths. One of the methods to integrate the advantages of a large exciton dissociation surface and direct charge transport pathways is to introduce ordered nanostructures into the BHJ system.

ZnO is an environmental friendly and low-cost semiconducting material with good air stability; especially, it is highly processable using low temperature solution-phase growth method [11,12] or printing/coating techniques on a range of substrates [13–16]. Successful use of ZnO nanostructures such as in the form of nanorods [17–22] and nano-ridges [23] as an electron transporter have been demonstrated. Those nanostructured ZnO patterns not only offer controllable transport path to direct electrons to reach the cathode but also serve as a hole blocker simultaneously. A power conversion efficiency (PCE) of PSC based on ZnO-nanorod (ZnO-NR) arrays in the most prominent photoactive system, poly(3-hexythiophene):(6,6)-phenyl C_{61} butyric acid methyl ester (P3HT:PCBM), has improved from 2.03% [18] to 3.56% [19] after including an anodic hole transport layer to modify the polymer/metal interface.

From the material perspective, the inorganic ZnO-NR/polymer interface is also problematic due to the different surface characters. The semiconducting ZnO-NRs tend to be hydrophilic while polymers are hydrophobic. Thus, it is essential and critical to manipulate the ZnO-NR surface character in order to obtain a good electrical coupling between these two classes of materials. A few research groups have intended to improve the ZnO-NR surface property for a better compatibility with organics based on various influences. Mercurochrome ($C_{20}H_8Br_2HgNa_2O$) [24] and N719 dye [25] were used to enhance the interfacial charge transport; alkanethiols were employed to modulate the crystalline order of the polymer [26]; mixing molecules of octyltrimethoxysilane and aminopropyltrimethoxysilane were selected to

* Corresponding authors.
E-mail addresses: fangchi@nuu.edu.tw (F.-C. Hsu).
yfchen@ntu.edu.tw (Y.-F. Chen).

0927-0248/$ - see front matter © 2012 Elsevier B.V. All rights reserved.
http://dx.doi.org/10.1016/j.solmat.2012.08.001

control the surface energy of the ZnO film for a rich photoactive layer morphology [27]. Though these surface modifiers function differently, the ultimate goal is to improve the performance of the solar cells. Unfortunately, these reported surface modifiers are either unfriendly to the environment or insulating against charge transport.

In this paper, we synthesize a relatively lower-cost and metal-free conductive molecule, an amine- and bromine-terminated 3-hexyl thiophene oligomer (oligo-3HT–(Br)NH_2, O3HT-NH_2) to adsorb on the ZnO-NR surface in an inverted hybrid ITO/ZnO-NR/P3HT:PCBM/Ag solar cell configuration. Our chosen oligomer is specially designed to have dual functions. The amino terminated functional group of the oligomer provides good affinity toward ZnO. At the same time, the oligomer contains approximately 20 repeating units having the same chemical structure as the light-harvesting conducting polymer, P3HT, which gives better interfacial compatibility between polymer blend and ZnO-NRs. This conjugated O3HT-NH_2 oligomer is able to passivate the ZnO-NR surface and prevent the back transfer of electrons for its large spatial dimension. Additionally, in the presence of the O3HT-NH_2 molecule, the electron mobility of the hybrid increases while higher hole concentration reaches the anodic surface for collection. The result indicates a modulation of microscopic morphology of bi-carrier transport pathways toward a more ordered and efficient configuration. Hence, the power conversion efficiency of the modified photovoltaic cells enhances as a result of improved photocurrent and photovoltage.

2. Experimental details

The chemical structure of oligo-3HT-(Br)NH_2 is shown in Fig. 1(a). The oligo-3HT-(Br)NH_2 (Mw=3.438 KDa, PDI=3.21) was synthesized by Grignard reaction [28,29], a kind of living polymerization. The molecular weight of the oligmer was controlled by the molar ratio of monomer to Ni catalyst in the feed. Briefly, in a three-neck round bottom flask, monomer: 2,5-dibromo-3-hexylthiophene 1 (3.26 g, 10.0 mmol) was dissolved in tetrahydrofuran (THF) (200 mL) and stirred under N_2. *tert*-Butylmagnesium chloride (5.0 mL, 10.0 mmol) was added via a syringe, and the mixture was stirred at reflux for 1 h. The nickel catalyst, Ni(dppp)Cl_2 (2.25 mol%) was added in one portion. The mixture was stirred for 10 min at room temperature, and the Grignard reagent 3-(bis[trimethylsilyl]amino)phenylmagnesium chloride (20–30 mol% of monomer) was added via a syringe to the reaction mixture. The mixture was stirred for additional 2 min and then poured into methanol to precipitate the oligomer. The oligomer was filtered and put into extraction thimble. The oligomer was purified by Soxhlet extraction with methanol and toluene overnight. The oligomer was obtained by the precipitating out of the toluene extract after adding methanol. The amino functional group terminated oligomer was characterized by ^{1}H-NMR at chemical shifts of 0.913 ppm (t, 3H), 1.40 ppm (m, 6H), 1.69 ppm (t, 2H), 2.80 ppm (t, 2H), 6.90 ppm(m, 0.05H), 6.98 ppm (s, 0.95H), 7.08 ppm (s, 0.036H)and 7.13 ppm (m, 0.016H) using TMS as standard.

Poly(3-hexythiophene) (P3HT, Mw=40 kDa, PDI=1.3, *RR*=99.5%) and (6,6)-phenyl C_{61} butyric acid methyl ester (PCBM) were purchased from Lumtech Ltd. Co. (Taiwan) and were used as received. We mention here that the molecular weight and molecular weight distribution of oligomer and polymer were determined using a Waters GPC (Breeze system). The system was equipped with two Waters Styragel columns (HR3 and HR4E), a refractive index detector (Waters 2414), and a dual-wavelength absorbance detector (Waters 2487). The apparatus was calibrated using polystyrene standards (Waters) and THF used as an eluent at 35 °C.

Initially, a ZnO seed layer (ca. 17 nm in thickness) was spin-coated on the pre-patterned indium tin oxide (ITO) coated glass from a 0.35 M solution of zinc acetate dehydrate (Ridel-de Hagën) in the cosolvents of monoethanolamine (Merck) and 2-methoxyethanol (Acros) [30] at a rate of 3000 rpm. The film was then annealed at 200 °C for an hour to remove the residual organic solvents. The oriented ZnO-NR arrays were subsequently grown from the ZnO seed-coated substrates by using the hydrothermal method [31]. The resulting ZnO-NRs are ~120 nm in length with an average diameter and rod-to-rod distance of 30 nm and 20–40 nm, respectively.

The oriented ZnO-NR arrays were subsequently immersed in 1.3×10^{-4} M O3HT-NH_2 anhydrous toluene solution at 60 °C in an oven for overnight followed by depositing the photoactive layer on top of the resulting structure. The active layer was formed by spin-coating the 40 mg mL^{-1} solution of P3HT:PCBM at 1:0.8 weight ratio in dichlorobenezene at a rate of 400 rpm. The thickness of the resulting films was ~200 nm. The solar cell was then completed by thermally depositing a silver layer (~100 nm) on top of the photoactive layer. Typical device active areas defined by the overlapping of ITO and silver electrodes are 4.0 mm^2.

The transmission electron microscopy (TEM) images were acquired on a FEI field-emission TEM, Tecnai F20, operated at 200 kV. The infrared spectral changes were determined at room temperature with a Perkin–Elmer Spectrum 1000 Fourier transform infrared spectroscopy (FTIR) system by a conventional method with a single cell. The photoluminescence (PL) spectroscopy was performed using a Jobin Yvon spec-1403 spectral system working in the double-grating mode. Kelvin probe force microscopy (KFM) measurements were performed in dark and under illumination of a halogen lamp (Royal Philips Electronics, 139, 50W) by Veeco Instruments Multimode AFM with an extended electronics module operating in the lift mode (typical lift height 20 nm) by a silicon cantilever with a PtIr surface coating. The charge extraction in linearly increasing voltage (CELIV) measurement was conducted in dark through a Textronic Model AFG3101 function generator to generate input voltage ramp pulses and the response signals were recorded simultaneously from a load in series to the photovoltaic cell using an Aligent Model DSO5054A oscilloscope. The current–voltage (*J–V*) characteristics of the finished solar cell devices were evaluated using a Keithley Model 2400 source meter under illumination intensity of 100 mW/cm^2 from a solar simulator (Newport Inc.) with AM 1.5 G filter. The incident photon-to-current conversion efficiency (IPCE) spectra were performed with a setup consisting of a lamp system, a chopper, a monochromator, a lock-in amplifier, and a standard silicon photodetector (ENLI Technology). All the characterizations were carried out in air at room temperature.

3. Results and discussion

Fig. 1(b) shows the TEM image of the adsorption of O3HT-NH_2 on ZnO-NRs surface. The dark contrast is the ZnO, which is revealed by the inset selected-area electron diffraction (SAED) pattern, indicating that the obtained ZnO-NR is monocrystalline and with wurtzite-type structure and oriented in *c*-axis direction; i.e., [0001] direction. A few nanometer thick O3HT-NH_2 layer covers the ZnO-NR surface as indicated by the arrows. The thickness of the adsorbed layer ranges from 1.5 to 5 nm (Fig. 1(c)), which may be due to the contour length distribution of O3HT-NH_2 molecule of an averaged MW of 3.438 KDa with a high PDI of 3.21. Apparently, the incubation of ZnO-NR arrays in O3HT-NH_s solution results in a monolayer of O3HT-NH_2 absorbing on ZnO-NR surface instead of a film deposited on ZnO-NR arrays. Fig. 1(d) depicts the FTIR spectra taken from 500 to 3500 nm for ZnO-NR arrays before and after immersed in toluene-based O3HT-NH_2 solution. After immersion, the spectrum

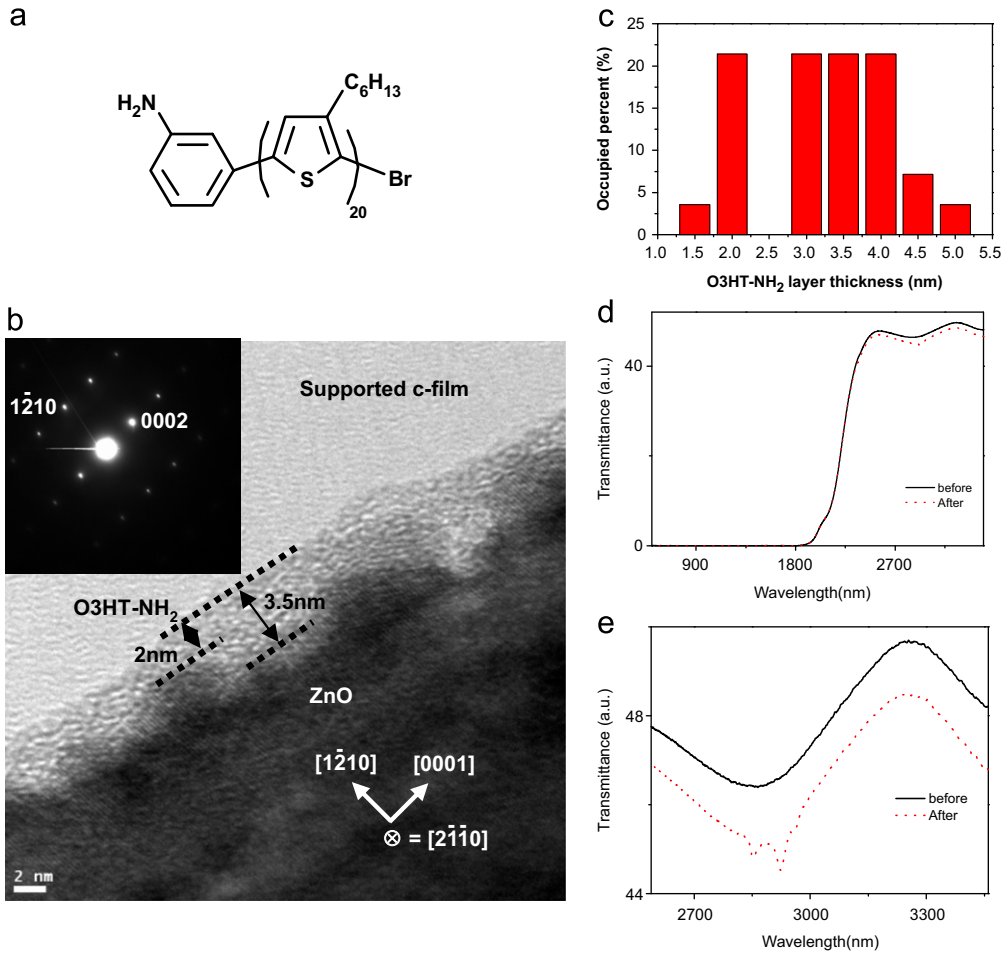

Fig. 1. (a) Chemical structure of O3HT-NH_2, (b) TEM image of O3HT-NH_2 adsorbing on ZnO-NR surface with inset SAED patterns of the ZnO–NR obtained from the dark portion of the image, (c) the thickness statistics for the O3HT-NH_2 layer on ZnO-NRs and (d) FTIR spectra for ZnO-NRs before and after O3HT-NH_2 immersion taken from 500 to 3500 nm with the zoom in region from 2800 to 3500 nm shown in (e).

shows no change of the transmission intensity except in the region of 2850–3000 nm (see Fig. 1(e)). There are three abrupt reduction bands around 2850, 2925, and 2963 nm. These are the typical CH stretching features, which can be attributed to the vibration of the methylene groups of the O3HT-NH_2 molecule [32,33]. The obtained alkyl side chain vibration characteristics suggest the adsorption of O3HT-NH_2 molecules on the ZnO-NR surface forming the ZnO-NR/O3HT-NH_2 structure.

The effect of O3HT-NH_2 adsorbed on ZnO-NR surface can be understood by photoluminescence (PL) spectroscopy. As seen in Fig. 2, the PL spectrum of pristine ZnO-NRs exhibits a sharp and a relatively broad luminescence peaks centered at 375 and 550 nm, respectively. The sharp and the broad peaks result from the band-to-band and defect band-to-band recombination of excited carriers in ZnO-NR arrays, respectively. These two categories of carrier relaxation routes display the comparable irradiation intensity. After a layer of O3HT-NH_2 adsorbing on ZnO-NR surface, the irradiation intensity of the former is stronger than that of the latter suggesting a reduction of surface defect concentration. The existence of O3HT-NH_2 on ZnO-NR surface can therefore effectively passivate the surface for lower surface defect status.

Since the incorporation of O3HT-NH_2 layer can reduce the surface defect density, we employ the Kelvin probe force microscopy (KFM) measurements [34–36] to gain more insight of the charge conduction influenced by the modification layer. We probe the relative surface potential (RSP) both in dark and under illumination for ZnO-NR/P3HT:PCBM and ZnO-NR/O3HT-NH_2/

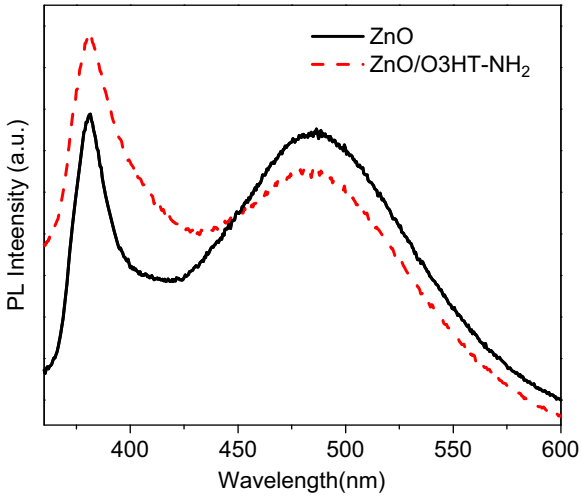

Fig. 2. PL spectra for ZnO-NRs before and after O3HT-NH_2 modification.

P3HT:PCBM structures on a 2 μm × 3 μm surface area. In a dark environment, both images are composed of brighter and darker domains, which correspond to the local Fermi level alignment of the P3HT-rich and PCBM-rich regions with the underneath ZnO-NR/ITO structure, respectively [37]. Particularly, the RSP distribution in dark for O3HT-NH_2-free structure is relatively

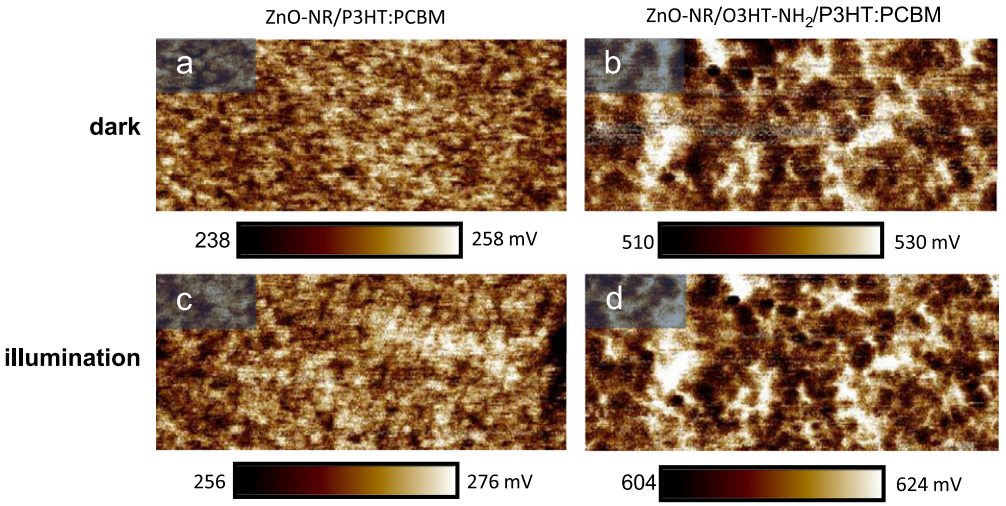

Fig. 3. KFM images showing the surface potential distribution for ZnO-NR/P3HT:PCBM structure in dark (a) and under illumination (c) as well as that for ZnO-NR/O3HT-NH_2/P3HT:PCBM configuration in dark (b) and under illumination (d).

homogeneous (see Fig. 3(a)) while that for the modified one presents the scatter of large fiber-like brighter blocks (see Fig. 3 (b)). The obtained RSP across the measured surface area are 238–258 mV for the former and 510–530 mV for the latter.

Upon illumination, the photogenerated excitons diffuse in P3HT phase and dissociate at the P3HT/PCBM or P3HT/ZnO-NR interfaces. Electrons migrate to the bottom ITO electrode through PCBM/ZnO-NR path and holes diffuse toward the top surface (anodic surface) through P3HT regions. The enhanced contrast within the KFM image reveals the final result of charge transport after exciton dissociation within the film. The measured RSPs for ZnO-NR/P3HT:PCBM and ZnO-NR/O3HT-NH_2/P3HT:PCBM are 256–276 mV (Fig. 3(c)) and 604–624 mV (Fig. 3(d)), respectively. The RSPs for both structures shift positively as compared to the values in dark showing the accumulation of extra positive charges on the surface under illumination. The average shifts of RSP under illumination are 18 (before) and 94 meV (after). The relatively large positive shift of RSP after modification reveals an increase in hole concentration reaching the top surface to be extracted to the anode, a result supporting the reduced free carrier loss from being trapped or recombined at the ZnO-NRs due to the reduction of the surface defect states.

On the other hand, Zeng et al. [38] point out that the enhanced RSP correlates with the improvement in the surface charge density and its mobility. We deposited a silver layer on top of the polymer blend to complete the photovoltaic cells and those devices were used directly for mobility measurements. Fig. 4 presents the device mobility measurement results by employing the charge-extraction-from-the-linear-increasing-voltage (CELIV) method [39–42]. The input voltage ramp pulses were from −0.35 to 2 V over a period of 40 μs and the corresponding current responses for devices before and after O3HT-NH_2 modification were recorded (see Fig. 4). Based on the recorded current transients, we calculated the individual carrier mobility (μ) by using $\mu=2d^2/[3t_{max}^2\ (1+0.36\Delta j(t=t_{max})/j(t=0))]$ [40], where d, t_{max}, $\Delta j(t=t_{max})$ and $j(t=0)$ stand for the device thickness, time period required for maximum extraction current, the maximum extraction current ($\Delta j(t=t_{max})$), and the capacitive displacement current ($j(t=0)$), respectively. The device mobilities were estimated to be 9.7×10^{-5} (before) and 2.6×10^{-4} $cm^2/V\,s$ (after). In a BHJ system, CELIV technique probes the mobility of more mobile species or both if their values are comparable [43]. Baumann et al. [44] pointed out that the electron mobility

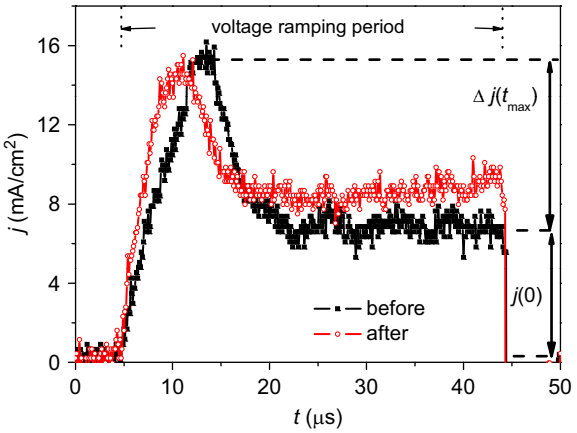

Fig. 4. Charge extraction transient for solar cell devices before and after O3HT-NH_2 modification obtained by using CELIV method.

($\sim10^{-4}$ $cm^2/V\,s$) is 10-fold higher than the hole mobility in the P3HT:PCBM blend. Thus, we assign the only carrier type detected here to be the electron. The hole mobility could be improved after O3HT-NH_2 treatment, but the improvement is not large enough to have the same order of magnitude as electron to be detected in the measuring time window of the technique used. The incorporating of O3HT-NH_2 molecule on ZnO-NR surface enhances the electron mobility by almost 3-fold.

The intermixing of the donor and acceptor materials forms a three-dimensional interpenetration network system. Electrons and holes travel in the respective network for conduction. The morphology of the network correlates with the transport property of the carrier and can be characterized by carrier mobility. Since there is a 3-fold enhancement in the electron mobility, the morphology of the electron conduction network is expected to be altered; hence, its counterpart, the hole conduction one, should respond accordingly. The change of BHJ morphology is also supported by the differences in RSP distribution features in dark as well as under light illumination. Several reports have shown that a BHJ system of more balanced charge transport properties [45–47] is important to reduce charge storage in the BHJ system. Unbalanced charge transport results in accumulation of slower charge species within the BHJ. Since larger hole concentration diffuse to the anodic surface for extraction, the nanomorphology

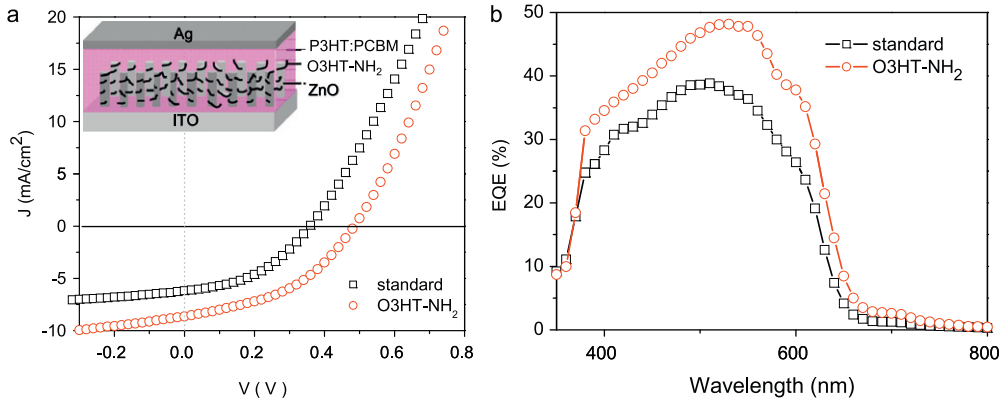

Fig. 5. (a) The *J*–V characteristics of the solar devices before and after O3HT-NH_2 modification under one sun illumination with AM 1.5 G filter. The schematic photovoltaic cell structure is shown in the inset. (b) EQE spectra for standard and O3HT-NH_2 treated devices.

of the bi-carrier transport networks of the hybrid is thus modulated toward a more efficient charge transport configuration.

Based on the schematic solar cell configuration shown in the inset in Fig. 5(a), we evaluate and compare the device performance before and after the O3HT-NH_2 modification under one sun irradiation with AM 1.5 G filter and the obtained *J*–*V* characteristics are shown in Fig. 5(a). The short circuit current (J_{SC}), open circuit voltage (V_{OC}), fill factor (*FF*), and PCE for device before modification are 6.0 mA/cm^2, 0.40 V, 0.42, and 1.28%, respectively, while those for the modified one are 8.8 mA/cm^2, 0.49 V, 0.40, and 1.73%, respectively. The presence of O3HT-NH_2 on the surface of ZnO-NR results in ~46% and ~22% increments in J_{SC} and V_{OC}, respectively, while *FF* remains. Both the photocurrent and photovoltage improvement enhance the device performance up to 35%. Fig. 5(b) depicts the corresponding EQE spectra for both devices. The EQE values for the modified device enhance over the entire measured wavelength regime. As an example, an EQE value of 38.8% at a wavelength of 510 nm for the standard device increases to 47.7% after O3HT-NH_2 treatment. The difference of the underneath area reflects the additional extracted charges observed in J_{SC} enhancement.

The improved device performance can be understood as follows. As described above, the O3HT-NH_2 layer reduces the defect density on the ZnO-NR surface, enhances carrier mobilities, and promotes the formation of a more efficient charge transport BHJ configuration such that the photo-generated free carriers can reach the respective electrodes for collection at their maximum capacity leading to J_{SC} improvement. It was reported [48,49] that the large spatial dimension of the surface modifier can effectively block the back transfer of electrons to compensate holes on the polymer backbone resulting in a decrease in interfacial recombination events. The conductive oligomer of ~20 repeat units used in this study is considered as a large molecule for its naturally coil form and can have good blocking ability on back transfer recombination, which may account for the photocurrent enhancement as well. In addition to reduced surface trapped charges on ZnO-NR surface, the large enhancement of free carriers in the constituent phase enlarges the *quasi*-Fermi level separation leading to improved V_{OC}. Additionally, the O3HT-NH_2 molecules could possibly fill up or cover pinholes in the ZnO seed layer to prevent direct contact of P3HT from ITO electrode [20]. This pinhole blocking effect can contribute to V_{OC} improvement as well.

The molecular weight of O3HT-NH_2 used has a large PDI of 3.21. We did not put special effort to synthesize the oligomer with low PDI. However, the PDI of the oligomer can be reduced by solvent extraction. Usually, the lower molecular weight conjugated oligomer exhibits lower conductivity. With a high PDI oligomer, the conductivity of the oligomer will be limited by the lower molecular weight molecule in the oligomer. However, in our study, the oligomer with a PDI of 3.21 serves as the purpose to reduce the recombination of electron and hole and to facilitate the charge transport. We have also tried to use O3HT-NH_2 of higher molecular weight (MW ~5.6 KDa) to modify the solar cell and the resulting device does not perform as well as the one modified by the lower MW. The dependency of solar cell performance on the MW of the surface modifier is worth of further study, and is among our ongoing research.

We stress here that the surface modifier used in this study is a metal-free conjugated oligomer of relatively lower cost as compared to the metal-containing conductive compound reported in the literature. Our selection of surface modifier improves the compatibility between the inorganic metal oxide and the organic blend leading to an apparent modulation in the microscopic mixing result of the polymer blend. The bi-carrier transport pathways become more ordered and are of greater carrier transport efficiency. The finding provides a least expensive and useful alternative to overcome the organic–inorganic interfacial problems.

4. Summary

We synthesize a metal-free conductive oligomer composed of a short segment structure of the light-harvesting polymer to adsorb on the ZnO-NR surface. This conjugated oligomer passivates the ZnO-NR surface for its adsorption activity. In addition, in the presence of this oligomer layer, the contacting BHJ blend with its microscopic morphology resulting from dual substance mixing is altered as suggested by the improved charge transport properties and the different features of KFM images. The nanomorphology manipulation effect induced by the metal-free conjugated surface modifier is also a major factor for the performance improvement of the photovoltaic cells. Our result shown here therefore provides an excellent key step for the application of hybrid organic–inorganic solar cells.

Acknowledgment

Authors would like to thank Mr. Sz-Chian Liou and Dr. Ming-Wen Chu of Center for Condensed Mater Science of Nation Taiwan University for helping with the TEM images. This work is supported by the National Science Council, Taiwan (Project nos. NSC 98-2112-M-239-001-MY3 and NSC 101-2112-M-239-001).

References

[1] F.C. Krebs, S.A. Gevorgyan, J. Alstrup, A roll-to-roll process to flexible polymer solar cells: model studies, manufacture, and operational stability studies, Journal of Materials Chemistry 19 (2009) 5442–5451.

[2] F.C. Krebs, M. Jørgensen, K. Norrman, O. Hagemann, J. Alstrup, T.D. Nielsen, J. Fyenbo, K. Larsen, J. Kristensen, A complete process for production of flexible large area polymer solar cells entirely using screen printing—first public demonstration, Solar Energy Materials and Solar Cells 93 (2009) 422–441.

[3] W.U. Huynh, J.J. Dittmer, A.P. Alivisatos, Hybrid nanorod–polymer solar cells, Science 295 (2002) 2425–2427.

[4] W. Ma, C. Yang, X. Gong, K. Lee, A.J. Heeger, Thermally stable, efficient polymer solar cells with nanoscale control of the interpenetrating network morphology, Advanced Functional Materials 15 (2005) 1617–1622.

[5] H.Y. Chen, J. Hou, S. Zang, Y. Liang, G. Yang, Y. Yang, L. Yu, Y. Wu, G. Li, Polymer solar cells with enhanced open-circuit voltage and efficiency, Nature Photonics 3 (2009) 649–653.

[6] J.H. Hou, H.Y. Chen, S.Q. Zhang, R.I. Chen, Y. Yang, Y. Wu, G. Li, Synthesis of a low band gap polymer and its application in highly efficient polymer solar cells, Journal of the American Chemical Society 131 (2009) 15586–15587.

[7] S.H. Park, A. Roy, S. Beaupre, S. Cho, N. Coats, J.S. Moon, D. Moses, M. Leclerc, K. Lee, A.J. Heeger, Bulk heterojunction solar cells with internal quantum efficiency approaching 100%, Nature Photonics 3 (2009) 297–303.

[8] Y.Y. Liang, Z. Xu, J.B. Xia, S.T. Tsai, Y. Wu, G. Li, C. Ray, L.P. Yu, For the bright future-bulk heterojunction polymer solar cells with power conversion efficiency of 7.4%, Advanced Materials 22 (2010) E135–E138.

[9] V.D. Mihailetchi, H.X. Xie, B. de Boer, L.J.A. Koster, P.W.M. Blom, Charge transport and photocurrent generation in poly(3-hexylthiophene):methanofullerene bulk heterojunction solar cells, Advanced Functional Materials 16 (2006) 699–708.

[10] G. Li, V. Shrotriya, J.S. Huang, Y. Yao, T. Moriarty, K. Emery, Y. Yang, High-efficiency solution processable polymer photovoltaic cells by self-organization of polymer blends, Nature Materials 4 (2005) 864–868.

[11] M.S. White, D.C. Olson, S.E. Shaheen, N. Kopidakis, D.S. Ginley, Inverted bulk-heterojunction organic photovoltaic device using a solution-derived ZnO underlayer, Applied Physics Letters 89 (2006) 143517-1–143517-3.

[12] A.K.K. Kyaw, X.W. Sun, C.Y. Jiang, G.Q. Lo, D.W. Zhao, D.L. Kwong, An inverted organic solar cell employing a sol–gel derived ZnO electron selective layer and thermal evaporated MoO_3 hole selective layer, Applied Physics Letters 93 (2009) 221107-1–221107-3.

[13] F.C. Krebs, T.D. Nielsen, J. Fyenbo, M. Wadstrøm, M.S. Pedersen, Manufacture, integration and demonstration of polymer solar cells in a lamp for the "Lighting Africa" initiative, Energy and Environmental Science 3 (2010) 512–525.

[14] F.C. Krebs, T. Tromholt, M. Jørgensen, Upscaling of polymer solar cell fabrication using full roll-to-roll processing, Nanoscale 2 (2010) 873–886.

[15] F.C. Krebs, Polymer solar cell modules prepared using roll-to-roll methods: knife-over-edge coating, slot-die coating and screen printing, Solar Energy Materials and Solar Cells 93 (2009) 465–475.

[16] F.C. Krebs, All solution roll-to-roll processed polymer solar cells free from indium-tin-oxide and vacuum coating steps, Organic Electronics 10 (2009) 76–768.

[17] P. Ravirajan, A.M. Peiró, M.K. Nazeeruddin, M. Gräetzel, D.D.C. Bradley, J.R. Durrant, J. Nelson, Hybrid polymer/zinc oxide photovoltaic devices with vertically oriented ZnO nanorods and an amphiphilic molecular interface layer, Journal of Physical Chemistry B 110 (2006) 7635–7639.

[18] D.C. Olson, J. Piris, R.T. Collins, S.E. Shaheen, D.S. Ginley, Hybrid photovoltaic devices of polymer and ZnO nanofiber composites, Thin Solid Films 496 (2006) 26–29.

[19] J.S. Huang, C.Y. Chou, M.Y. Liu, K.H. Tsai, W.H. Lin, C.F. Lin, Solution-processed vanadium oxide as an anode interlayer for inverted polymer solar cells hybridized with ZnO nanorods, Organic Electronics 10 (2009) 1060–1065.

[20] K. Takanezawa, K. Hirota, Q. Wei, K. Tajima, K. Hashimoto, Efficient charge collection with ZnO annorod array in hybrid photovoltaic devices, Journal of Physical Chemistry C 111 (2007) 7218–7223.

[21] A.M. Peiró, P. Ravirajan, K. Govender, D.S. Boyle, P. O'Brien, D.D.C. Bradley, J. Nelson, J.R. Durrant, Hybrid polymer/metal oxide solar cells based on ZnO nanocolumnar structure, Journal of Materials Chemistry 16 (2006) 2088–2096.

[22] C.T. Chen, F.C. Hsu, S.W. Kuan, Y.F. Chen, The effects of C_{60} on ZnO-nanorod surface in organic–inorganic hybrid photovoltaics, Solar Energy Materials and Solar Cells 95 (2011) 740–744.

[23] N. Sekine, C.H. Chou, W.L. Kwan, Y. Yang, ZnO nanoridge structure and its application in inverted polymer solar cell, Organic Electronics 10 (2009) 1473–1477.

[24] Y.Y. Lin, Y.Y. Lee, L. Chang, J.J. Wu, C.C. Chen, The influence of interface modifier on the performance of nanostructured ZnO/polymer hybrid solar cells, Applied Physics Letters 94 (2009) 063308-1–063308-3.

[25] R. Thitima, C. Patcharee, S. Takashi, Y. Susumu, Efficient electron transfers in ZnO nanorod arrays with N719 dye for hybrid solar cells, Solid-State Electronics 53 (2009) 176–180.

[26] T.C. Monson, M.T. Lloyd, D.C. Olson, Y.J. Lee, J.W.P. Hsu, Photocurrent enhancement in polythiophene and alkanethiol-modified ZnO solar cells, Advanced Materials 20 (2008) 4755–4759.

[27] X. Bulliard, S.G. Ihn, S. Yun, Y. Kim, D. Choi, J.Y. Choi, M. Kim, M. Sim, J.H. Park, W. Choi, K. Cho, Enhanced performance in polymer solar cells by surface energy control, Advanced Engineering Materials 20 (2010) 438–4387.

[28] R.S. Loewe, S.M. Khersonsky, R.D. McCullough, A simple method to prepare head-to-tail coupled, regioregular poly(3-alkylthiophenes) using Grignard metathesis, Advanced Materials 11 (1999) 250–253.

[29] M. Jeffries-El, G. Sauvé, R.D. McCullough, Facile synthesis of end-functionalized regioregular poly(3-alkylthiophene)s via modified Grignard metathesis reaction, Macromolecules 38 (2005) 10346–10352.

[30] M. Ohyama, H. Kozuka, T. Yoko, Sol–gel preparation of ZnO films with extremely preferred orientation along (002) plane from zinc acetate solution, Thin Solid Films 306 (1997) 78–85.

[31] L. Vayssieres, Growth of arrayed nanorods and nanowires of ZnO from aqueous solutions, Advanced Materials 15 (2003) 464–466.

[32] Y.D. Park, D.H. Kim, Y. Jang, J.H. Cho, M. Hwang, H.S. Lee, J.A. Lim, K. Cho, Effect of side chain length on molecular ordering and field-effect mobility in poly(3-alkylthiophene) transistors, Organic Electronics 7 (2006) 514–520.

[33] X.M. Jiang, C.O. Au, R. Österbacka, Z.V. Vardeny, FTIR studies of charged photoexcitations in region-regular and region-random poly(3-alkylthiophene) films, Synthetic Metals 16 (2001) 203–206.

[34] V. Palermo, M. Palma, P. Samorì, Electronic characterization of organic thin films by Kelvin probe microscopy, Advanced Materials 18 (2006) 145–164.

[35] M.C. Wu, Y.J. Wu, W.C. Yen, H.H. Lo, C.F. Lin, W.F. Su, Correlation between nanoscale surface potential and power conversion efficiency of P3HT/TiO2 nanorod bulk heterojunction photovoltaic devices, Nanoscale 2 (2010) 1448–1454.

[36] Y.M. Sung, F.C. Hsu, D.Y. Wang, I.S. Wang, C.C. Chen, H.C. Liao, W.F. Su, Y.F. Chen, Enhanced charge extraction in inverted hybrid photovoltaic cells assisted by graphene nano-flakes, Journal of Materials Chemistry 21 (2011) 17462–17467.

[37] K. Maturová, M. Kemerink, M.M. Wienk, D.S.H. Charrier, R.A.J. Janssen, Scanning Kelvin probe microscopy on bulk heterojunction polymer blends, Advanced Functional Materials 19 (2009) 1379–1386.

[38] T.W. Zeng, F.C. Hsu, Y.C. Tu, T.H. Lin, W.F Su, Kelvin probe force microscopy study on hybrid P3HT:titanium dioxide nanorod materials, Chemical Physics Letters 479 (2009) 105–108.

[39] G. Juška, K. Arlauskas, M. Viliūnas, J. Kočka, Extraction current transients: new method of study of charge transport in microcrystalline silicon, Physical Review Letters 22 (2000) 4946–4949.

[40] A.J. Mozer, N.S. Sarciftci, A. Pivrikas, R. Österbacka, G. Juška, L. Brassat, H. Bässler, Charge carrier mobility in regioregular poly (3-hexylthiophene) probed by transient conductivity techniques: a comparative study, Physical Review B 71 (2005) 035214-1–035214-9.

[41] A.J. Mozer, N.S. Sariciftci, L. Lutsen, D. Vanderzande, R. Österbacka, M. Westerling, G. Juška, Charge transport and recombination in bulk heterojunction solar cells studied by the photoinduced charge extraction in linearly increasing voltage technique, Applied Physics Letters 86 (2005) 112104-1–112104-3.

[42] Y.M. Sung, F.C. Hsu, C.T. Chen, W.F. Su, Y.F. Chen, Enhanced photocurrent and stability of inverted polymer/ZnO-nanorod solar cells by 3-hydroxyflavone additive, Solar Energy Materials and Solar Cells 98 (2012) 103–109.

[43] G. Juška, N. Nekrasas, K. Arlauskas, J. Stuchlik, A. Fejfar, J. Kočka, Photogenerated carriers in μc-Si:H/a-Si:H multi-layers, Journal of Non-Crystalline Solids 338–340 (2004) 353–356.

[44] A. Baumann, J. Lormann, C. Deibel, V. Dyakonov, Bipolar charge transport in poly(3-hexyl thiophene)/methanofullerene blends: a ration dependent study, Applied Physics Letters 93 (2008) 252104-1–252104-3.

[45] S. Wu, J. Li, Q. Tai, F. Yan, Investigation of high-performance air-processed poly(3-hexythiophene)/methanofullene bulk-heterojunction solar cells, Journal of Physical Chemistry C 114 (2010) 21873–21877.

[46] V.D. Mihailetchi, H. Xie, B. De Boer, L.J.A. Koster, P.W.M. Blom, Charge transport and photocurrent generation in poly(3-hexylthiophene):methanofullerene bulk-heterojunction solar cells, Advanced Functional Materials 16 (2006) 699–708.

[47] J. Huang, G. Li, Y. Yang, Influence of composition and heat-treatment on the charge transport properties of poly(3-hexylthiophnen) and [6,6]-phenyl C61-butyric acid methyl ester blends, Applied Physics Letters 87 (2005) 112105-1–112105-3.

[48] Y.Y. Lin, T.H. Chu, S.S. Li, C.H. Chuang, C.H. Chang, W.F. Su, C.P. Chang, M.W. Chu, C.W. Chen, Interfacial nanostructuring on the performance of polymer/TiO_2 nanorod bulk heterojunction solar cells, Journal of the American Chemical Society 131 (2009) 3644–3649.

[49] Y.C. Huang, J.H. Hsu, Y.C. Liao, W.C. Yen, S.S. Li, S.T. Lin, C.W. Chen, W.F. Su, Employing an amphiphilic interfacial modifier to enhance the performance of a poly(3-hexyl thiophene)/TiO_2 hybrid solar cell, Journal of Materials Chemistry 21 (12) (2011) 4450–4456.